NANO LETTERS

Letter

pubs.acs.org/NanoLett

Quantifying "Softness" of Organic Coatings on Gold Nanoparticles Using Correlated Small-Angle X-ray and Neutron Scattering

Benjamin T. Diroll,[†] Katie M. Weigandt,[‡] Davit Jishkariani,[†,§] Matteo Cargnello,[†,#] Ryan J. Murphy,[§] Lawrence A. Hough,[§] Christopher B. Murray,[*,†,∥] and Bertrand Donnio[*,§,⊥]

[†]Department of Chemistry, University of Pennsylvania, Philadelphia, Pennsylvania 19104, United States

[‡]NIST, Center for Neutron Research, National Institute of Standards and Technology, Gaithersburg, Maryland 20899-6102, United States

[§]Complex Assemblies of Soft Matter Laboratory (COMPASS), CNRS-SOLVAY—University of Pennsylvania, UMI 3254, CRTB, Bristol, Pennsylvania 19007, United States

[∥]Department of Materials Science and Engineering, University of Pennsylvania, Philadelphia, Pennsylvania 19104, United States

[⊥]Institut de Physique et Chimie des Matériaux de Strasbourg (IPCMS), CNRS—Université de Strasbourg, UMR 7504, 67034 Strasbourg cedex 2, France

Supporting Information

ABSTRACT: Small-angle X-ray and neutron scattering provide powerful tools to selectively characterize the inorganic and organic components of hybrid nanomaterials. Using hydrophobic gold nanoparticles coated with several commercial and dendritic thiols, the size of the organic layer on the gold particles is shown to increase from 1.2 to 4.1 nm. A comparison between solid-state diffraction from self-assembled lattices of nanoparticles and the solution data from neutron scattering suggests that engineering softness/deformability in nanoparticle coatings is less straightforward than simply increasing the organic size. The "dendritic effect" in which higher generations yield increasingly compact molecules explains changes in the deformability of organic ligand shells.

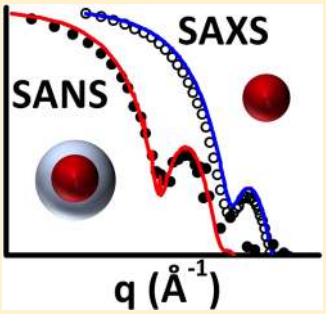

KEYWORDS: *Small-angle X-ray scattering, small-angle neutron scattering, dendrimer, self-assembly, superlattice, gold nanoparticles*

The combination of inorganic function with organic specificity underpins many applications of nanotechnology, including targeted biomedical therapies,[1−3] sensors,[4] metamaterials,[5] catalysis,[6] and energy conversion.[7] Magnetic, catalytic, radioactive, or optically active materials can now be functionalized with a wide variety of surfactants, polymers, covalently bound organic molecules, and biomolecules.[1,3,8] As might be expected from the functional orthogonality of organic/inorganic hybrids, methods for characterizing each elementary component of these hybrid materials are also typically orthogonal.

Although transmission electron microscopy (TEM) is by far the most common method for characterizing inorganic colloidal nanoparticles (NPs), small-angle X-ray scattering (SAXS) is the measurement *par excellence* to characterize the size and monodispersity of inorganic colloids. Unlike TEM, SAXS measures the ensemble properties: it is not prone to selection and exclusion biases, and the measurement may easily describe the material in colloidal solutions, rather than the solid state. But due to the substantially lower contrast of organic material, neither SAXS nor TEM are effective measurements for observing nanometer-scale organic layers on the surface of inorganic NPs. With neutrons, on the other hand, the contrast is not tied to atomic number and can depend heavily on isotope. This isotopic sensitivity is often harnessed as a tool for adjusting contrast, most notably by controlling the concentration of protium and deuterium in various components of a sample. This ability to vary contrast makes small-angle neutron scattering (SANS) an ideal complementary measurement to SAXS for the study of organic coatings and other mixed organic−inorganic systems. A combined approach of SAXS and SANS measurements provide valuable data for evaluating ensemble size, shape, and polydispersity of hybrid colloids including those used for biomedical applications in which there is low tolerance for batch or vendor differences.

SANS has been heavily used to study the formation and dynamics of micelles and polymers in solution. The combination of SAXS and SANS measurements has been used to analyze ligand dynamics, conformation, and thickness.[9−15] Recently, Gómez-Graña et al. demonstrated the use of SAXS and SANS analysis to determine the thickness of surfactant bilayers on the surfaces of gold nanorods.[10] Other work has used SANS exclusively to estimate the size, morphology, and dynamics of surfactant layers and surface-bound molecules.[16−21] Here, we extend the approach of

Received: August 12, 2015
Published: November 18, 2015

DOI: 10.1021/acs.nanolett.5b04011
Nano Lett. 2015, 15, 8008−8012

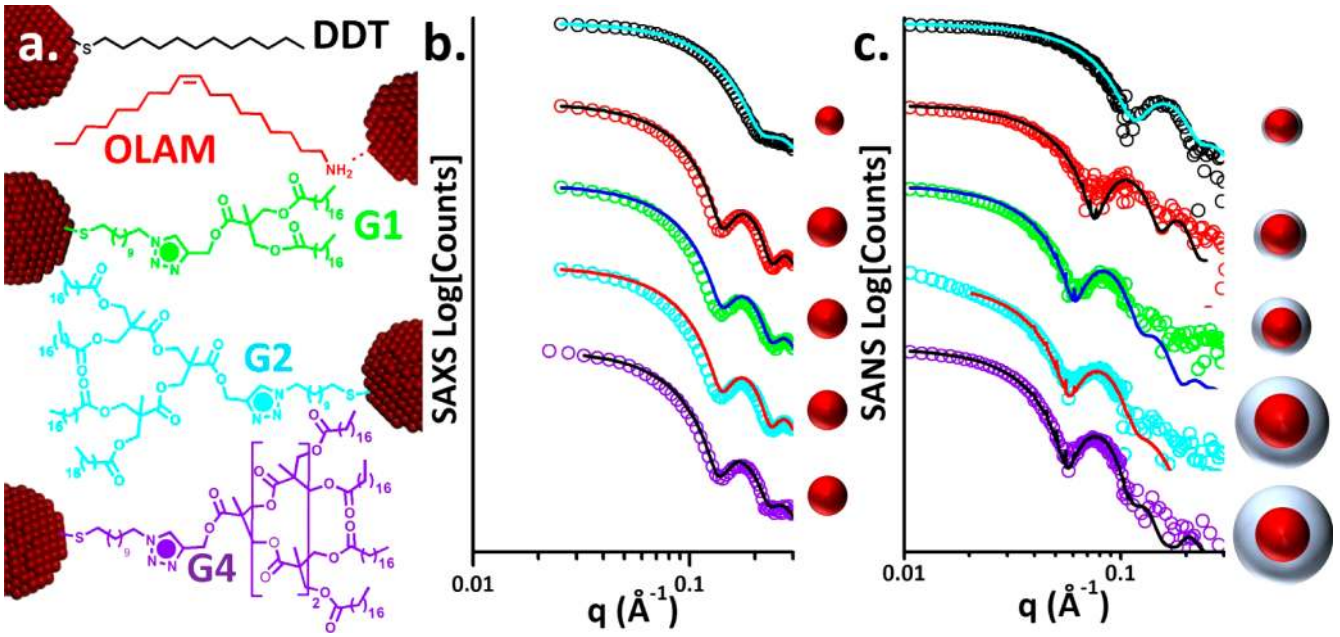

Figure 1. (a) Ligands used in this study on Au NPs. Ligands are color-coded according to the corresponding data in parts b and c. (b) SAXS data in open circles and fit lines for Au@L hybrids. Data are for L = DDT (black), L = OLAM (red), L = G1 (green), L = G2 (cyan), and L = G4 (violet). (c) SANS data for Au@L hybrids in contrast-matched toluene. SAXS and SANS data are shown after subtracting the solvent background from the data and the fitted background from fit curves.

correlated SAXS and SANS to study a series of hydrophobic ligand-coated gold hybrid NPs (Au@L) in which the organic monolayer thickness in solution is gradually controlled from 1.2 nm with the common commercial ligand dodecanethiol (L = DDT) to 4.1 nm by the synthesis of disulfide dendritic molecules with one (L = G1), two (L = G2), and four (L = G4) generations. The synthesis of these thiol wedges was based on 2,2-bis(hydroxymethyl)propionic acid (bis-MPA) and each branch was terminated with stearic acid groups, as described recently.[22] (See Scheme S1 and Figure S1 in the Supporting Information.)

Previously, we demonstrated that these dendronized hybrid materials offer systematic, tunable interparticle spacing in the solid state and that they can be crystallized into single-component and binary superlattice structures analogous to atomic crystals.[22] They are therefore an excellent system for measuring variable organic coronae of inorganic NPs and for comparing the dimensions of solvated species with those in dry solids—i.e. to quantify the "softness" or deformability of the organic component of a hybrid system. To synthesize Au@L hybrid systems, oleylamine-stabilized Au NPs (Au@OLAM) were first synthesized by reduction of chloroauric acid[24] followed, after purification, by ligand-exchange with disulfide dendrimers. This procedure results in effective functionalization of the Au NP with the desired ligand molecules, verified by NMR.[22] Unbound ligands were removed through three steps of precipitation and redispersion of the Au@L hybrids. Figure 1a shows each of the molecules, which are used in this study. (Full structures are shown in Supporting Information Figure S1.) The corresponding SAXS patterns of Au@L hybrids are shown in Figure 1b with a fit curve shown with a solid line. A standard analytical model is used to fit the data:[25]

$$I(q) = \frac{S}{V_c}\left[\frac{3V_c(\rho_c - \rho_{sol})(\sin[qr_c] - qr_c\cos[qr_c])}{(qr_c)^3}\right]^2 + B$$

Here, S is a scaling factor proportionate to the number of nanoparticles, V_c is the volume of the Au core and not an independent variable, and ρ_c and ρ_{sol} are X-ray scattering length densities (SLD) of the core (calculated as 125 Å^{-2}) and solvent (calculated as 6.8 Å^{-2}). r_c is the radius of a spherical core, which is fit as a Gaussian distribution consistent with TEM (see Supporting Information, Figure S2), and B is the isotropic background. In the absence of precise definition of the SLD of the core and solvent, this difference is subsumed into the scaling prefactor, which is proportional to the volume fraction, without affecting estimates of the NP size and polydispersity. That is, the scaling factor and SLD difference in both X-ray and neutron measurements are highly correlated and therefore only scale is permitted to float in our fitting.

SANS data were fitted with a spherical core/shell model in which the radius and size dispersion of the core are fixed by SAXS measurements. Experiments were performed at contrast matching conditions in toluene, in which the neutron SLD of the solvent and core are matched at the SLD of gold (4.5×10^{-6} Å^{-2}). The core/shell model takes the form[25]

$$I(q) = \frac{S}{V_s}\left[\frac{3V_c(\rho_c - \rho_s)(\sin[qr_c] - qr_c\cos[qr_c])}{(qr_c)^3} + \frac{3V_s(\rho_s - \rho_{sol})(\sin[qr_s] - qr_c\cos[qr_s])}{(qr_s)^3}\right]^2 + B$$

in which terms for the SLD (ρ_s), volume (V_s), and radius (r_s) of the spherical shell are added. During fitting, ρ_s was fixed at -1×10^{-7} Å^{-2}, the SLD of stearic acid dissolved in a deuterated benzene solution.[26] This SLD represents the average SLD of solvated stearic acid, which represents the majority of the organic ligand shell in our dendritic systems, and therefore is a reasonable approximation of the SLD expected from the organic ligands on the NP surface. The assumed SLD value is not precisely accurate for each ligand, but if the scaling factor S

DOI: 10.1021/acs.nanolett.5b04011
Nano Lett. 2015, 15, 8008−8012

Table 1. Sample Fitting Results and Geometrical Data

coating, L	r_c (nm)[a]	t_s (nm)[b]	γ[c]	crystal	a (nm)[d]	graft density (nm^{-2})[e]	peripheral alkyl density (nm^{-2})[f]	linear contraction (%)[g]	Voronoi volume/solution volume[h]
DDT	2.0 ± 0.3	1.2 ±0.2	0.6	fcc	8.1	5.8	2.2	26	0.99
OLAM	3.2 ± 0.2	1.7 ± 0.2	0.5	hcp	8.8	4.2	1.8	29	0.97
G1	3.2 ± 0.2	3.3 ± 0.4	1.0	hcp	11.1	2.5	1.2	31	0.79
G2	3.3 ± 0.2	3.7 ± 0.6	1.1	hcp	11.9	1.6	1.4	27	0.82
G4	3.2 ± 0.3	4.1 ± 0.2	1.3	hcp	13.6	0.7	2.2	13	1.09

[a]Au core radius, from SAXS. [b]Shell thickness, $t_s = r_s - r_c$, calculated from SAXS and SANS. [c]$\gamma = t_s/r_c$.[23] [d]Unit cell a parameter. [e]Values deduced from thermogravimetric analysis measurements.[22] [f]Chain density (number/area) at the periphery of the organic shell in solution. [g]Percent difference of edge-to-edge spacing and t_s. [h]Volume of *organic* Voronoi polyhedron in the solid state (minus inorganic sphere) divided by the volume of the organic shell in solution. Explanation of the calculation is given in the Supporting Information. The +/− values represent 1 standard deviation in error.

is permitted to float in the fitting process, it is sufficient that the SLD of the organic shell is distinct from solvent (4.5×10^{-6} $Å^{-2}$) to obtain information on the size of the organic layer. Both the scale and background terms are refit for SANS data with fixed SLD values and fixed core size and polydispersity.

The findings of this correlated fitting procedure are shown in Figure 1, parts b and c. In Figure 1b, X-ray patterns for five samples of Au NP are shown in colored scattered plots offset for clarity with fits in solid lines. The average inorganic diameter of the NPs obtained from the fitting procedure is included next to the plot and in Table 1. SANS data is shown in the same colors for the same samples in Figure 1c. Comparing the SAXS and SANS data shows a clear shift of the oscillatory features to lower q values, indicating that the size of the species scattering neutrons is larger than the structures analyzed by SAXS measurements.

The extent of this shift depends on the organic coating. Figure 1c shows data in which the organic coating is progressively larger. DDT and OLAM, common commercial reagents for hydrophobic NPs with only a single alkane chain, show organic coatings of 1.2 and 1.7 nm, respectively, which are very similar to previous measurements of dodecanethiol and octadecanethiol ligands on Au NPs in good solvents and oleic acid ligands on PbSe/CdSe core/shell NPs.[13,16,21] The dendritic ligands with two (G1, 3.3 nm), four (G2, 3.7 nm), and 16 stearate chains (G4, 4.1 nm) generate progressively thicker organic coatings. Using the same size of Au core (e.g., 6 nm), the solvated volume of the Au@L hybrids can be increased by a factor of 5 across the series of ligands used in this study.

Monodisperse Au@L hybrids can be used as the building blocks for single-component and binary superlattices by slow evaporation of colloidal solutions.[22] TEM images of single-component superlattices are shown in Figures 2, parts a and b. Figure 2c shows the SAXS patterns of the dried films for the five hybrids for which solution data are shown in Figure 1. In addition to the oscillatory patterns also apparent in Figure 1, an additional structure factor can be observed from many peaks in the SAXS patterns. The fitted structures, either *hcp* layers, formed from epitaxy on the surface, or *fcc* crystals are reported in Table 1 with the relevant unit cell parameters. In some cases, both close-packed structures are possibly in evidence, but only one is reported here.

Previous work by Boles and Talapin suggested that "softer" systems—defined as those with larger organic volume fractions—facilitate packing of self-assembled structures.[23] One mechanism proposed for the improved packing behavior of softer ligands was that the organic coatings of hydrophobic NPs can deform from the spherical core/shell structure

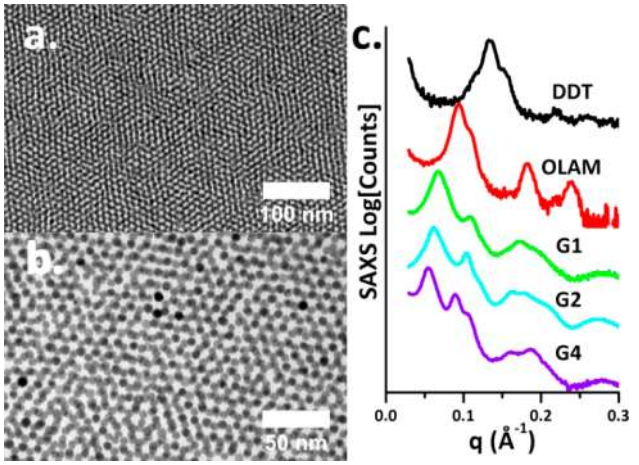

Figure 2. TEM micrographs of superlattices composed of (a) Au@G1 and (b) Au@G2 hybrids. (c) SAXS data of dried Au@L films.

observed of the solvated state to a Voronoi polyhedron in the solid state (Wigner−Seitz cell), yielding a higher packing fraction. Other recent work has claimed that the formation of *bcc*-type superlattices of NPs in such systems is due to a minimization of ligand packing frustration.[27] Interdigitation of ligands should also be noted as a potential mechanism of enhanced packing. A comparison of the solid-state SAXS data with the solvated SANS data for the samples of our study suggests that this may be less straightforward than previously thought. Table 1 offers three figures of merit for the "softness" of a NP-ligand hybrid. For comparison, we have listed the softness parameter (γ) defined by Boles and Talapin, but measured based upon a comparison of solution SAXS and SANS data, in Table 1. Assuming an incompressible Au fraction, the contraction or softness of spheres from the solvated state when dried into a NP superlattices is attributed solely to contraction of the organic shell. This contraction may be evaluated in one dimension—changes in the near-neighbor spacing reflecting bending of ligands from the interface of two spheres—or three dimensions, from the perspective of space-filling.

The linear contraction of the samples is reported in Table 1 as a percentage change of the organic shell length from the solvated state measured in SANS experiments to edge-to-edge spacing measured in the solid state. The largest dendron, with 16 stearate chains, shows the smallest contraction (13%) of the organic shell. Each of the other samples shows very similar contractions, between 26 and 31%. Contraction and deformation is described in three dimensions by comparing

DOI: 10.1021/acs.nanolett.5b04011
Nano Lett. 2015, 15, 8008−8012

the relative size of the Voronoi polyhedron of each Au NP with the size of the organic volume in solution. This ratio does not necessarily imply that space-filling reaches 100% (or higher), but it provides a measure of relative deformability or softness. Lower values of this ratio imply that the ligand shell deforms more effectively to fill space. Au@DDT and Au@OLAM hybrids have very similar values close to 1. The Au@G1 and Au@G2 hybrids show greater deformability, consistent with their lower peripheral alkyl chain densities. Again, Au@G4 stands out as particularly "hard": unlike other samples, the solvated size of the organic shell is smaller than the organic volume of the polyhedron necessary for complete space-filling in the solid state.

These measurements indicate that "softness" defined by the relative size of the organic material does not necessarily lead to greater flexibility of the organic ligands in the solid state. Rather, the route by which softer materials are obtained is also important: linear extensions of alkyl groups for molecules with similar graft densities lead to an organic layer with comparatively lower density and greater flexibility.[23,28] This effect is observed particularly in the relative deformability in three dimensions of the Au@G1 and Au@G2 hybrids, which have the lowest peripheral alkyl chain densities. But using a dendritic ligand, in which branching of alkyl chains extends the organic coating but retains or even increases the density, can yield diminishing or even negative returns in the softness or deformability of the organic layer, as seen in the Au@G4 hybrid. In fact, this phenomenon is already well-known as a "dendritic effect": although the particulars depend on the terminating group and branching connectivity (degree of branching, junctions, and spacing), higher generations of dendrimer typically demonstrate more dense, less compressible structures than lower generations or linear analogs.[29−34] We conclude from these experiments that the tendency for higher generations of dendrimers toward reduced compressibility is also operative in the packing of surface-bound dendritic ligands of Au@L hybrids and that this congestion effect can even drive self-assembly into more open structures overall.

The combination of SAXS and SANS measurements not only provides Angstrom-scale size resolution for hybrid nanomaterials but also offers a window to study the response of each element of a hybrid system to external stimuli. Our findings suggest that many of the heuristics for the swelling and mechanical properties of polymer chemistry can be applied to complex "soft" ligands grafted on to colloidal NPs. Although demonstrated here for a hydrophobic material with dendritic ligands, these techniques and analysis can be applied to a wide variety of hybrid systems with molecular, polymeric, or biological coatings in both aqueous and nonaqueous environments.

■ ASSOCIATED CONTENT

Supporting Information

The Supporting Information is available free of charge on the ACS Publications website at DOI: 10.1021/acs.nanolett.5b04011.

Experimental details (PDF)

■ AUTHOR INFORMATION

Corresponding Authors

*(C.B.M.) E-mail: cbmurray@sas.upenn.edu.
*(B.D.) E-mail: bdonnio@ipcms.unistra.fr.

Present Address

#Department of Chemical Engineering, Stanford University.

Notes

The authors declare no competing financial interest.

■ ACKNOWLEDGMENTS

This work was supported by the CNRS-UPENN-SOLVAY through the Complex Assemblies of Soft Matter Lab. (COMPASS), in partnership with Penn's NSF MRSEC under Award No. DMR-112090. SANS work was conducted on the 10 m SANS line at the NIST Center for Neutron Research, supported in part by the nSoft Consortium. This work benefited from SasView software, originally developed by the DANSE project under NSF Award No. DMR-0520547. C.B.M. acknowledges the Richard Perry University Professorship at the University of Pennsylvania. B.D. acknowledges additional support from the ANR Programme blanc, METABIP, 12BS10-003.

■ REFERENCES

(1) Sperling, R. A.; Parak, W. J. *Philos. Trans. R. Soc., A* **2010**, *368*, 1333−1383.
(2) Na, H. B.; Song, I. C.; Hyeon, T. *Adv. Mater.* **2009**, *21*, 2133−2148.
(3) Bruchez, M., Jr.; Maronne, M.; Gin, P.; Weiss, S.; Alivisatos, A. P. *Science* **1998**, *281*, 2013−2016.
(4) Nam, J.-M.; Thaxton, C. S.; Mirkin, C. A. *Science* **2003**, *301*, 1884−1886.
(5) Fafarman, A. T.; Hong, S.-H.; Caglayan, H.; Ye, X.; Diroll, B. T.; Paik, T.; Engheta, N.; Murray, C. B.; Kagan, C. R. *Nano Lett.* **2013**, *13*, 350−357.
(6) Han, Z.; Qiu, F.; Eisenberg, R.; Holland, P. L.; Krauss, T. D. *Science* **2012**, *338*, 1321−1324.
(7) Ip, A. H.; Thon, S. M.; Hoogland, S.; Voznyy, O.; Zhitomirsky, D.; Debnath, R.; Levina, L.; Rollny, L. R.; Carey, G. H.; Fischer, A.; Kemp, K. W.; Kramer, I. J.; Ning, Z.; Labelle, A. J.; Chou, K. W.; Amassian, A.; Sargent, E. H. *Nat. Nanotechnol.* **2012**, *7*, 577−582.
(8) Medintz, I. L.; Uyeda, H. T.; Goldman, E. R.; Mattoussi, H. *Nat. Mater.* **2005**, *4*, 435−446.
(9) Draper, M.; Saez, I. M.; Cowling, S. J.; Gai, P.; Heinrich, B.; Donnio, B.; Guillon, D.; Goodby, J. W. *Adv. Funct. Mater.* **2011**, *21*, 1260−1278.
(10) Gómez-Graña, S.; Hubert, F.; Testard, F.; Guerrero-Martínez, A.; Grillo, I.; Liz-Marzán, L. M.; Spalla, O. *Langmuir* **2012**, *28*, 1453−1459.
(11) Thomson, T.; Lee, S. L.; Toney, M. F.; Dewhurst, C. D.; Ogrin, F. Y.; Oates, C. J.; Sun, S. *Phys. Rev. B: Condens. Matter Mater. Phys.* **2005**, *72*, 064441.
(12) Kim, C. J.; Sondergeld, K.; Mazurowski, M.; Gallei, M.; Rehahn, M.; Spehr, T.; Frielinghaus, H.; Stühn, B. *Colloid Polym. Sci.* **2013**, *291*, 2087−2099.
(13) Abel, K. A.; FitzGerald, P. A.; Wang, T.-Y.; Regier, T. Z.; Raudsepp, M.; Ringer, S. P.; Warr, G. G.; van Veggel, F. C. J. M. *J. Phys. Chem. C* **2012**, *116*, 3968−3978.
(14) Dulle, M.; Jaber, S.; Rosenfeldt, S.; Radulescu, A.; Förster, S.; Mulvaney, P.; Karg, M. *Phys. Chem. Chem. Phys.* **2015**, *17*, 1354−1367.
(15) Yang, W.; Lu, J.; Gilbert, E. P.; Knott, R.; He, L.; Cheng, W. *J. Phys. Chem. C* **2015**, *119*, 18773−18778.
(16) Von White, G.; Kitchens, C. L. *J. Phys. Chem. C* **2010**, *114*, 16285−16291.
(17) Mehan, S.; Chinchalikar, A. J.; Kumar, S.; Aswal, V. K.; Schweins, R. *Langmuir* **2013**, *29*, 11290−11299.
(18) Johnson, J. A.; Saboungi, M.-L.; Thiyagarajan, P.; Csencsits, R.; Meisel, D. *J. Phys. Chem. B* **1999**, *103*, 59−63.
(19) Jia, H.; Grillo, I.; Titmuss, S. *Langmuir* **2010**, *26*, 7482−7488.
(20) Shen, L.; Stachowiak, A.; Fateen, S. E. K.; Laibinis, P. E.; Hatton, T. A. *Langmuir* **2001**, *17*, 288−299.

DOI: 10.1021/acs.nanolett.5b04011
Nano Lett. 2015, 15, 8008−8012

(21) Von White, G.; Mohammed, F. S.; Kitchens, C. L. *J. Phys. Chem. C* **2011**, *115*, 18397−18405.
(22) Jishkariani, D.; Diroll, B. T.; Cargnello, M.; Klein, D. R.; Hough, L. A.; Murray, C. B.; Donnio, B. *J. Am. Chem. Soc.* **2015**, *137*, 10728−10734.
(23) Boles, M. A.; Talapin, D. V. *J. Am. Chem. Soc.* **2015**, *137*, 4494−4502.
(24) Peng, S.; Lee, Y.; Wang, C.; Yin, H.; Dai, S.; Sun, S. *Nano Res.* **2008**, *1*, 229−234.
(25) Guinier, A.; Fournet, G. *Small-Angle Scattering of X-Rays*; John Wiley and Sons: New York, 1955.
(26) Eremin, R. A.; Kholmurodov, K. T.; Petrenko, V. I.; Rosta, L.; Avdeev, M. V. *Phys. Solid State* **2014**, *56*, 81−85.
(27) Goodfellow, B. W.; Yu, Y.; Bosoy, C. A.; Smilgies, D.-M.; Korgel, B. A. *J. Phys. Chem. Lett.* **2015**, *6*, 2406−2412.
(28) Hadar, I.; Abir, T.; Halivni, S.; Faust, A.; Banin, U. *Angew. Chem., Int. Ed.* **2015**, *54*, 12463−12467.
(29) Hawker, C. J.; Malmstrom, E. E.; Frank, C. W.; Kampf, J. P. *J. Am. Chem. Soc.* **1997**, *119*, 9903−9904.
(30) Förster, S.; Neubert, I.; Schlüter, A. D.; Lindner, P. *Macromolecules* **1999**, *32*, 4043−4049.
(31) Mansfield, M. L. *Macromolecules* **2000**, *33*, 8043−8049.
(32) Mallamace, F.; Canetta, E.; Lombardo, D.; Mazzaglia, A.; Romeo, A.; Scolaro, L. M.; Maino, G. *Phys. A* **2002**, *304*, 235−243.
(33) Maiti, P. K.; Çağin, T.; Wang, G.; Goddard, W. A. *Macromolecules* **2004**, *37*, 6236−6254.
(34) Rathgeber, S.; Monkenbusch, M.; Kreitschmann, M.; Urban, V.; Brulet, A. *J. Chem. Phys.* **2002**, *117*, 4047−4062.

DOI: 10.1021/acs.nanolett.5b04011
Nano Lett. 2015, 15, 8008−8012